The Eigenvector-Eigenvalue Identity Applied to Fast Calculation of polSAR Scattering Characterization

Allan Aasbjerg Nielsen

***Abstract*— Unlike the original Cloude–van Zyl decomposition of reflection symmetric polarimetric synthetic aperture radar (polSAR) data, a recently suggested version of the decomposition for full/quad pol data relies on the Cloude–Pottier mean alpha angle ($\bar{\alpha}$) to characterize the scattering mechanism. $\bar{\alpha}$ can be calculated from the eigenvectors of the coherency matrix. By means of the eigenvector-eigenvalue identity (EEI), we can avoid the calculation of the eigenvectors. The EEI finds $\bar{\alpha}$ by means of eigenvalues of the 3 × 3 coherency matrix and its 2 × 2 minor(s) only and is well suited for fast array-based computer implementation. In this letter with focus on computational aspects, we demonstrate fast EEI-based determination of $\bar{\alpha}$ on X-band Flugzeug synthetic aperture radar (F-SAR) image data over Vejers, Denmark, including a detailed example of calculations and computer code.**

***Index Terms*— Anisotropy, coherency matrix, complex covariance matrix, entropy, Flugzeug synthetic aperture radar (F-SAR), Hermitian matrix, mean alpha angle ($\bar{\alpha}$), polarimetric synthetic aperture radar (polSAR), X-band.**

I. Introduction

In THE covariance matrix formulation of multilook polarimetric synthetic aperture radar (polSAR) image data each pixel is described by a complex 3 × 3 matrix

$$\boldsymbol{C} = \begin{bmatrix} \langle S_{hh} S_{hh}^* \rangle & \sqrt{2}\langle S_{hh} S_{hv}^* \rangle & \langle S_{hh} S_{vv}^* \rangle \\ \sqrt{2}\langle S_{hv} S_{hh}^* \rangle & 2\langle S_{hv} S_{hv}^* \rangle & \sqrt{2}\langle S_{hv} S_{vv}^* \rangle \\ \langle S_{vv} S_{hh}^* \rangle & \sqrt{2}\langle S_{vv} S_{hv}^* \rangle & \langle S_{vv} S_{vv}^* \rangle \end{bmatrix}.$$

This matrix is Hermitian also known as self-adjoint, i.e., the matrix is equal to its own conjugate transpose, $\boldsymbol{C} = \boldsymbol{C}^H$, the superscript ^{H} denotes transpose and complex conjugate (which is denoted by *), $\langle\rangle$ denotes ensemble averaging. The trace, the determinant, and all eigenvalues are real and nonnegative.

The Hermitian coherency matrix is $\boldsymbol{T} = \boldsymbol{N}\boldsymbol{C}\boldsymbol{N}^T$ [1] where

$$\boldsymbol{N} = \frac{1}{\sqrt{2}} \begin{bmatrix} 1 & 0 & 1 \\ 1 & 0 & -1 \\ 0 & \sqrt{2} & 0 \end{bmatrix}.$$

The full/quad pol covariance matrix $\boldsymbol{C}$ and the coherency matrix $\boldsymbol{T}$ have the same eigenvalues.

The Cloude–Pottier decomposition [1], [2] of the coherency matrix $\boldsymbol{T}$ gives us entropy, H, anisotropy, A, and the mean alpha angle, $\bar{\alpha}$. The sorted eigenvalues of $\boldsymbol{T}$ are $\lambda_1 \geq \lambda_2 \geq \lambda_3$. As a measure of target disorder, entropy H is defined as

$$H = -\sum_{i=1}^{3} p_i \log_3 p_i \quad \text{with} \quad p_i = \frac{\lambda_i}{\sum_{i=1}^{3} \lambda_i}$$

$0 \leq H \leq 1$. Low entropy is associated with a single dominant scattering mechanism, high entropy with random scattering.

Manuscript received March 1, 2022; revised April 7, 2022; accepted April 20, 2022. Date of publication April 22, 2022; date of current version May 12, 2022.

The author is with the DTU Compute, Department of Applied Mathematics and Computer Science, Technical University of Denmark, 2800 Lyngby, Denmark (e-mail: alan@dtu.dk).

Digital Object Identifier 10.1109/LGRS.2022.3169994

Anisotropy A can be considered a measure of departure from azimuthal symmetry and is defined as

$$A = \frac{\lambda_2 - \lambda_3}{\lambda_2 + \lambda_3}$$

$0 \leq A \leq 1$. Low anisotropy is associated with azimuthal symmetry.

Fast array-based calculation of eigenvalues for 3 × 3 (and 2 × 2) Hermitian matrices is described in [3].

The eigenvectors $\boldsymbol{e}_i, i = 1, 2, 3$, of $\boldsymbol{T}$ are of the form

$$\boldsymbol{e}_i = \exp(j\phi_i) \begin{bmatrix} \cos\alpha_i \\ \sin\alpha_i \cos\beta_i \exp(j\delta_i) \\ \sin\alpha_i \sin\beta_i \exp(j\gamma_i) \end{bmatrix}$$

where α_i, β_i, δ_i, and γ_i are angles which characterize the scattering. Note that the angle ϕ_i is arbitrary: $\boldsymbol{e}_i$ may be rotated by any angle ϕ_i, i.e., $\boldsymbol{e}_i$ may be replaced by $\boldsymbol{e}_i \exp(j\phi_i)$ and still be a solution to the eigenproblem.

Here, we are interested in the α_i only. For the squared norm $|e_{i1}|^2$ of the first component e_{i1} of $\boldsymbol{e}_i$ we have

$$\begin{aligned} |e_{i1}|^2 &= \exp(j\phi_i)\cos\alpha_i \exp(-j\phi_i)\cos\alpha_i \\ &= \cos^2\alpha_i \end{aligned}$$

(the squared norm is independent of the arbitrary rotation angle ϕ_i). For $\bar{\alpha}$, we have

$$\bar{\alpha} = \sum_{i=1}^{3} p_i \alpha_i \quad \text{with} \quad \alpha_i = \arccos|e_{i1}|.$$

$\bar{\alpha} = 0°$ is associated with single bounce (surface) scattering, $\bar{\alpha} = 45°$ with scattering from differently oriented dipoles (typically vegetation), and $\bar{\alpha} = 90°$ with (conductive) double bounce scattering.

Calculating eigenvectors is more cumbersome than calculating eigenvalues, and it seems we need the first component of the eigenvectors to calculate the α_i and $\bar{\alpha}$. Sections II–V show that we can obtain these angles without the eigenvectors by means of the so-called eigenvector-eigenvalue identity (EEI) and give computationally oriented examples.

II. Eigenvector–Eigenvalue Identity

Let $\boldsymbol{H}$ be an $n \times n$ Hermitian matrix with eigenvalues $\lambda_1(\boldsymbol{H}) \geq \cdots \geq \lambda_n(\boldsymbol{H})$ and eigenvectors $\boldsymbol{e}_i$ (we reuse the symbols $\boldsymbol{e}_i$). We write e_{ij} for the jth component of $\boldsymbol{e}_i$. $\boldsymbol{H}$ has $(n-1) \times (n-1)$ minors $\boldsymbol{M}_j$, $j = 1, \ldots, n$, made from $\boldsymbol{H}$ by deleting the jth row and the jth column from $\boldsymbol{H}$. These minors are also Hermitian with eigenvalues $\lambda_1(\boldsymbol{M}_j) \geq \cdots \geq \lambda_{n-1}(\boldsymbol{M}_j)$. For these eigenvalues we have the so-called Cauchy interlacing inequalities

$$\lambda_i(\boldsymbol{H}) \geq \lambda_i(\boldsymbol{M}_j) \geq \lambda_{i+1}(\boldsymbol{H})$$

for $i = 1, \ldots, n-1$.

Fig. 1. Part of Vejers, Denmark, approximately the area covered by the F-SAR data, from Google Earth. We see (summer) houses, caravan sites with a swimming pool and service buildings (a grocery store and a petrol station), the main road called Vejers Havvej (where the text "Vejers" appears) going mostly east-west, dirt roads, vegetation, etc.

According to [4]–[6] we have the following so-called eigenvector-eigenvalue identity (EEI) for the squared norm $|e_{ij}|^2$ of the components of the eigenvectors $\boldsymbol{e}_i$

$$|e_{ij}|^2 \prod_{k=1,k\neq i}^{n} (\lambda_i(\boldsymbol{H}) - \lambda_k(\boldsymbol{H})) = \prod_{k=1}^{n-1} (\lambda_i(\boldsymbol{H}) - \lambda_k(\boldsymbol{M}_j)).$$

A related expression due to Jacobi appeared already in 1834.

As stated above the phase of any individual $\boldsymbol{e}_i$ is arbitrary, therefore the relative phase between e_{ik} and e_{jk}, $i \neq j$, is arbitrary. However, the relative phases between the components of any $\boldsymbol{e}_i$, say between e_{ij} and e_{ik} for $j \neq k$, is not arbitrary.

Despite the simple nature of the EEI and the mature state of development of linear algebra, this identity was not widely known until recently [6].

For the Cloude–Pottier decomposition of full/quad polSAR data, $\boldsymbol{H} = \boldsymbol{T}$, the 3×3 coherency matrix and the minor $\boldsymbol{M}_1$ comes from $\boldsymbol{T}$ by removing the first row and the first column, so $\boldsymbol{M}_1$ is 2×2. In this case, we get for the squared norm of the first component of each of the three eigenvectors

$$|e_{11}|^2 = \frac{(\lambda_1(\boldsymbol{T}) - \lambda_1(\boldsymbol{M}_1))(\lambda_1(\boldsymbol{T}) - \lambda_2(\boldsymbol{M}_1))}{(\lambda_1(\boldsymbol{T}) - \lambda_2(\boldsymbol{T}))(\lambda_1(\boldsymbol{T}) - \lambda_3(\boldsymbol{T}))}$$

$$|e_{21}|^2 = \frac{(\lambda_2(\boldsymbol{T}) - \lambda_1(\boldsymbol{M}_1))(\lambda_2(\boldsymbol{T}) - \lambda_2(\boldsymbol{M}_1))}{(\lambda_2(\boldsymbol{T}) - \lambda_1(\boldsymbol{T}))(\lambda_2(\boldsymbol{T}) - \lambda_3(\boldsymbol{T}))}$$

$$|e_{31}|^2 = \frac{(\lambda_3(\boldsymbol{T}) - \lambda_1(\boldsymbol{M}_1))(\lambda_3(\boldsymbol{T}) - \lambda_2(\boldsymbol{M}_1))}{(\lambda_3(\boldsymbol{T}) - \lambda_1(\boldsymbol{T}))(\lambda_3(\boldsymbol{T}) - \lambda_2(\boldsymbol{T}))}.$$

These expressions are well suited for fast array-based computer implementation. We obtain the α_i and $\bar{\alpha}$ from $|e_{i1}|$ as above in Section I, here without calculating the eigenvectors.

III. Image Data Example

In a project headed by the Danish Ministry of Defense Acquisition and Logistics Organization (DALO) the Flugzeug synthetic aperture radar (F-SAR) system of the German Aerospace Center (DLR) has been used to acquire data at several locations in Denmark and Greenland. The F-SAR offers the possibility of exploring the performance of a high resolution, fully polarimetric SAR system with five frequency bands in the range from ∼300 to ∼10 GHz [7].

The Cloude–Pottier decomposition is illustrated with airborne F-SAR X-band data (frequency 9.60 GHz corresponding to a wavelength of ∼3 cm). The data were acquired on 20 June 2017 covering a central part of the village Vejers on the Danish west coast, Fig. 1. The scene covers the east–west main road (called Vejers Havvej where the text "Vejers" appears in Fig. 1) going to and from the sea, campsites with caravans to the south of the road, a swimming pool, parking lots, and several service buildings (grocery store, petrol station, etc.) as well as many small and big houses north and south of the road. These

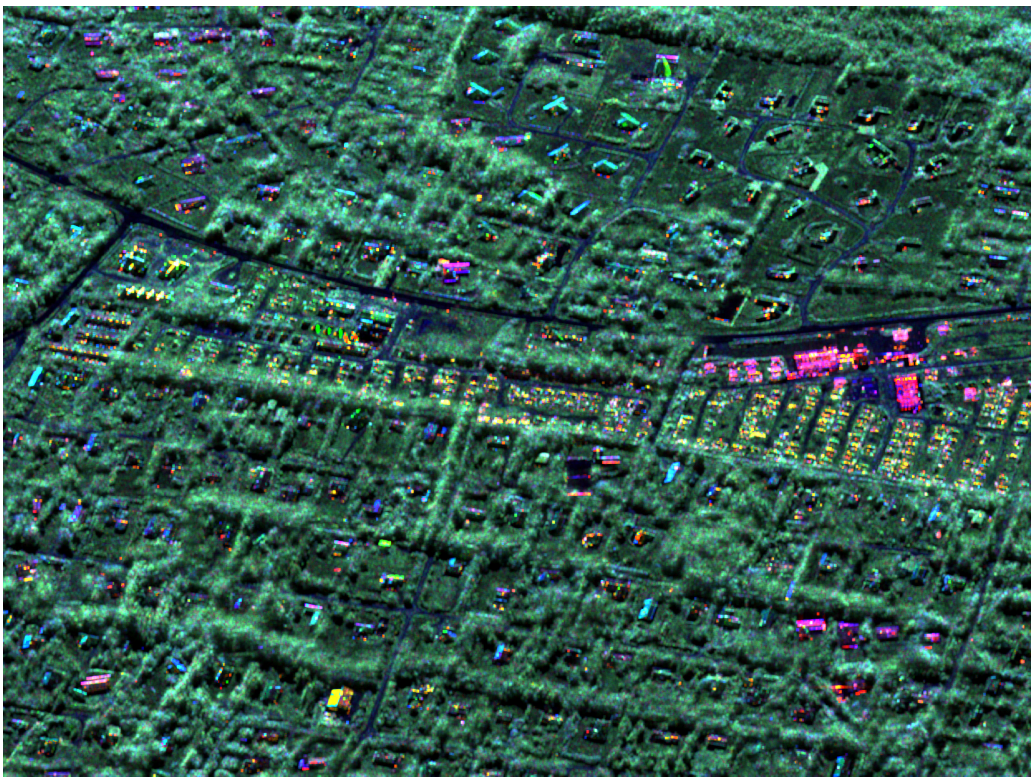

Fig. 2. Full/quad pol version of Cloude–van Zyl decomposition. Red objects are mainly buildings which are characterized by double bounce reflection. Green objects are mainly characterized by volume scattering (typically vegetation), or dihedral targets which are rotated with respect to the flight line which is east–west, here right-left, looking from north. Blue areas are mainly objects which are characterized by single bounce reflection. The yellow caravans, for example, are characterized both by double bounce and rotated dihedrals. Range increases from top to bottom of the image.

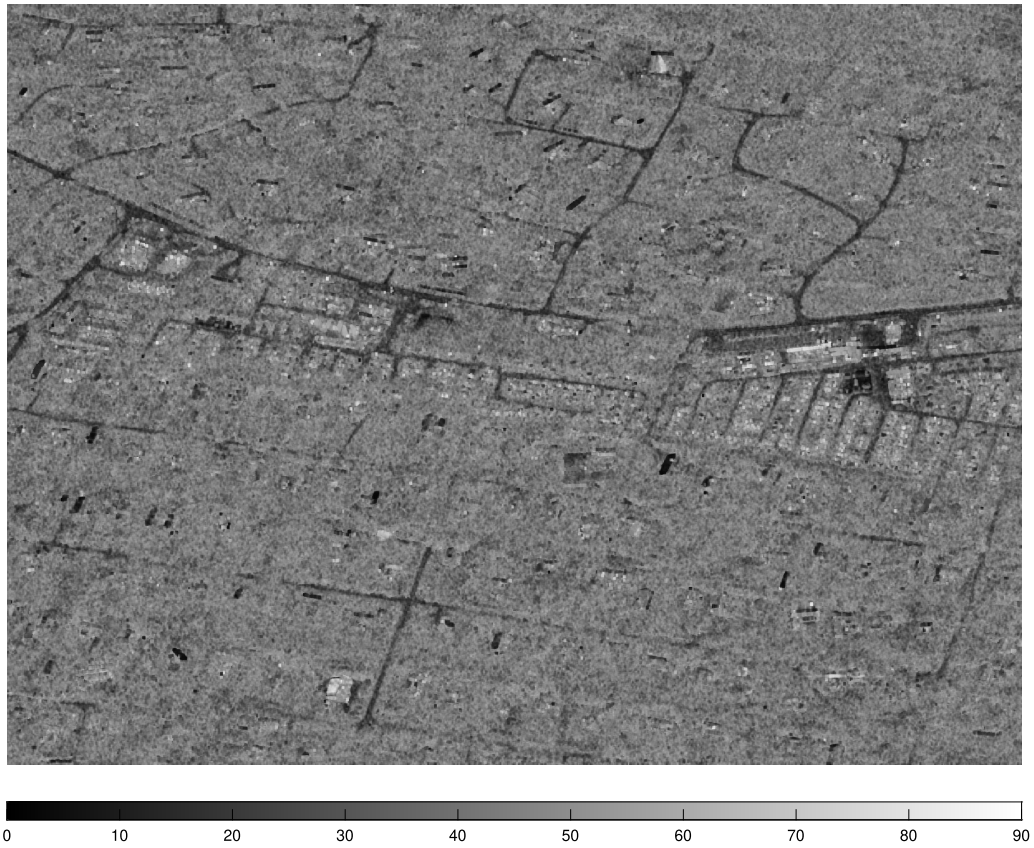

Fig. 3. Cloude–Pottier mean alpha angle, $\bar{\alpha}$ in degrees. In accordance with remarks in Section I and with Fig. 2, roads have low values for $\bar{\alpha}$, vegetation has $\bar{\alpha}$ around 45°, and parts of most of the buildings and caravans have very low or very high values (single or double bounce).

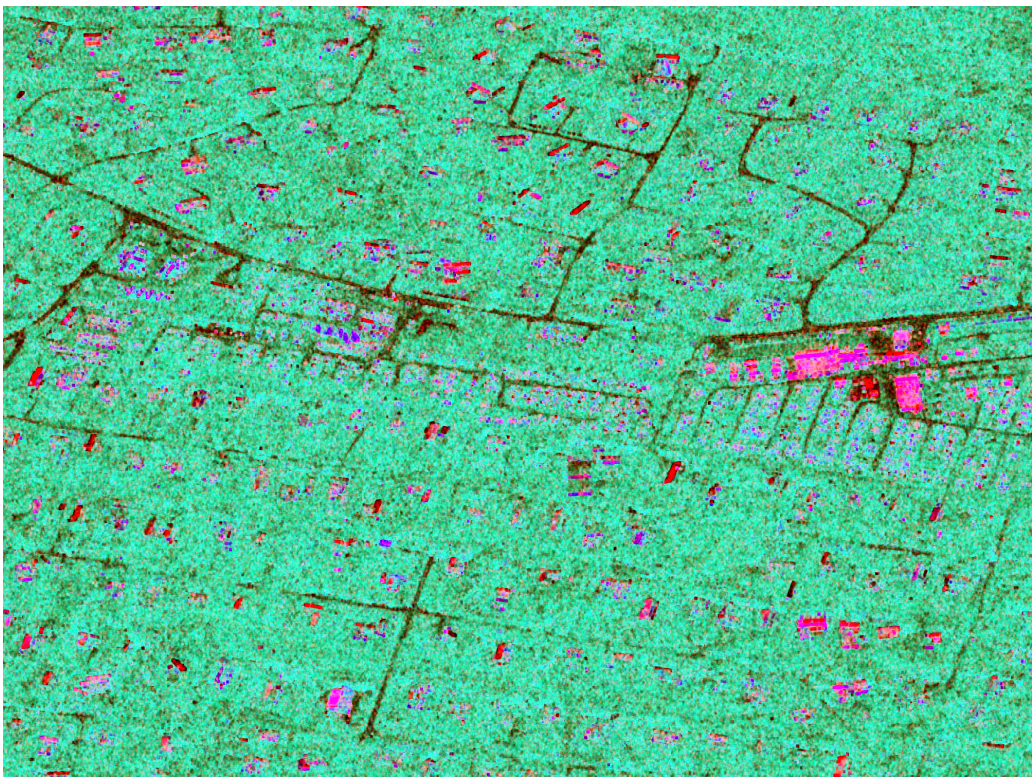

Fig. 4. RGB representation of the Cloude–Pottier decomposition of the coherency matrix. Red is anisotropy (A), green is entropy (H), blue is mean alpha angle ($\bar{\alpha}$). Man-made structures, mostly houses and caravans, appear red-magenta-purple-blue (i.e., high or intermediate values of A and/or $\bar{\alpha}$ with low values of H), vegetation green (i.e., high values of H with lower values of A and $\bar{\alpha}$), and roads black-dark gray (i.e., low values of all three parameters).

data are dealt with also in [8] which introduces a full/quad pol version of the (original, reflection symmetry-based) Cloude–van Zyl decomposition [9], [10].

Fig. 2 shows this full/quad pol version of the Cloude–van Zyl decomposition for a 3000 rows by 4800 columns scene. Red objects are mainly buildings which are characterized by double bounce reflection. Green objects are mainly characterized by volume scattering (typically vegetation), or dihedral targets which are rotated with respect to the flight line. Blue areas are mainly objects that are characterized by single bounce reflection. The yellow caravans, for example, are characterized both by double bounce and rotated dihedrals.

Fig. 3 shows the Cloude–Pottier mean alpha angle ($\bar{\alpha}$). In accordance with remarks in Section I and with Fig. 2, roads have low values for $\bar{\alpha}$, vegetation has $\bar{\alpha}$ around 45°, and parts of most of the buildings and caravans have very low or very high values (single or double bounce).

Fig. 4 shows anisotropy (A), entropy (H), and mean alpha angle ($\bar{\alpha}$) as red-green-blue (RGB). Man-made structures, mostly houses and caravans, appear red-magenta-purple-blue (i.e., high or intermediate values of A and/or $\bar{\alpha}$ with low values of H), vegetation green (i.e., high values of H with lower values of A and $\bar{\alpha}$), and roads black-dark gray (i.e., low values of all three parameters).

Array-based calculations take around 0.37 μs per pixel for determination of H, $\bar{\alpha}$ and A carried out in eight-byte precision with MATLAB R2022a on a MacBook Pro from 2019, 2.3 GHz 8-Core Intel i9 processor, 64 GB 2667 MHz DDR4 memory. This is a speed-up of a factor of ∼55 over an implementation with calls to MATLAB function svd in for-loops over all pixels.

IV. Worked EEI Example

For a detailed illustration of the EEI calculations, we select a pixel on a roof with double bounce ($H = 0.0573$, $\bar{\alpha} = 87.2°$ and $A = 0.6946$). For this pixel, we have covariance and coherency matrices as shown at the top of the next page. From MATLAB function eig, we get eigenvalues $\lambda_i(\boldsymbol{T})$ for $\boldsymbol{T}$ (first row above the horizontal line) and corresponding (column) eigenvectors $\boldsymbol{e}_i$

25.7837	0.2325	0.0419
$0.0206 - j0.0306$	$-0.9477 - j0.2958$	$-0.1084 - j0.0347$
$0.4709 - j0.8811$	$0.0347 + j0.0097$	$0.0151 - j0.0197$
-0.0234	-0.1141	0.9932

The eigenvectors from eig are rotated such that the third components are real. Based on these eigenvectors we get

$$\begin{aligned} |e_{11}|^2 &= (+0.0206 - j0.0306)(+0.0206 + j0.0306) \\ &= 0.0014 \\ |e_{21}|^2 &= (-0.9477 - j0.2958)(-0.9477 + j0.2958) \\ &= 0.9857 \\ |e_{31}|^2 &= (-0.1084 - j0.0347)(-0.1084 + j0.0347) \\ &= 0.0130. \end{aligned}$$

If we use MATLAB function svd instead, we get the same eigenvalues $\lambda_i(\boldsymbol{T})$ (first row above the horizontal line) and differently rotated corresponding (column) eigenvectors $\boldsymbol{e}_i$

25.7837	0.2325	0.0419
-0.0369	0.9928	0.1138
$-0.9938 + j0.1020$	$-0.0360 + j0.0011$	$-0.0084 + j0.0233$
$0.0131 + j0.0194$	$0.1089 - j0.0340$	$-0.9459 + j0.3029$

$$\boldsymbol{C} = \begin{bmatrix} 13.937 & -0.196 + j0.393 & -12.735 - j0.097 \\ -0.196 - j0.393 & 0.059 & 0.207 + j0.358 \\ -12.735 + j0.097 & 0.207 - j0.358 & 12.062 \end{bmatrix} = \begin{bmatrix} 13.9 & 0.4\exp(j116.4°) & 12.7\exp(-j179.6°) \\ 0.4\exp(-j116.4°) & 0.1 & 0.1\exp(j60.0°) \\ 12.7\exp(j179.6°) & 0.4\exp(-j60.0°) & 12.1 \end{bmatrix}$$

$$\boldsymbol{T} = \begin{bmatrix} 0.2648 & 0.9373 + j0.0967 & 0.0082 + j0.0249 \\ 0.9373 - j0.0967 & 25.7347 & -0.2847 + j0.5311 \\ 0.0082 - j0.0249 & -0.2847 - j0.5311 & 0.0585 \end{bmatrix} = \begin{bmatrix} 0.26 & 0.94\exp(j5.9°) & 0.03\exp(j71.8°) \\ 0.94\exp(-j5.9°) & 25.74 & 0.60\exp(j118.2°) \\ 0.03\exp(-j71.8°) & 0.60\exp(-j118.2°) & 0.06 \end{bmatrix}.$$

The eigenvectors from svd are rotated such that the first components are real. Based on these eigenvectors, we get

$$|e_{11}|^2 = (-0.0369)^2 = 0.0014$$
$$|e_{21}|^2 = (+0.9928)^2 = 0.9857$$
$$|e_{31}|^2 = (+0.1138)^2 = 0.0130$$

i.e., the same solution as the one based on eig. Rotation angles to obtain eigenvectors based on svd from eigenvectors based on eig are

$\boldsymbol{e}_1$	$\boldsymbol{e}_2$	$\boldsymbol{e}_3$
$-0.5589-j0.8292$	$-0.9546+j0.2980$	$-0.9524+j0.3050$
$=$	$=$	$=$
$\exp(-j124.0°)$	$\exp(j162.7°)$	$\exp(j162.2°)$

.

For the $\alpha_i = \arccos|e_{i1}|$ (or $\alpha_i = \cos^{-1}|e_{i1}|$), we get

$$\begin{bmatrix} \alpha_1 \\ \alpha_2 \\ \alpha_3 \end{bmatrix} = \begin{bmatrix} 87.8850° \\ 6.8722° \\ 83.4644° \end{bmatrix} \quad \text{with} \quad \begin{bmatrix} p_1 \\ p_2 \\ p_3 \end{bmatrix} = \begin{bmatrix} 0.9895 \\ 0.0089 \\ 0.0016 \end{bmatrix}$$

resulting in $\bar{\alpha} = 87.2°$.

$\boldsymbol{T}$ has first minor (delete first row and column from $\boldsymbol{T}$)

$$\boldsymbol{M}_1 = \begin{bmatrix} 25.7347 & -0.2847 + j0.5311 \\ -0.2847 - j0.5311 & 0.0585 \end{bmatrix}$$

with eigenvalues $\lambda_i(\boldsymbol{M}_1) = [25.7489\ 0.04438]$. Note that the Cauchy interlacing inequalities hold.

For the squared norm $|e_{i1}|^2$ of the first components e_{i1} of $\boldsymbol{e}_i$ the EEI gives

$$|e_{11}|^2 = \frac{(25.7837 - 25.7489)(25.7837 - 0.04438)}{(25.7837 - 0.2325)(25.7837 - 0.0419)} = 0.0014$$
$$|e_{21}|^2 = \frac{(0.2325 - 25.7489)(0.2325 - 0.04438)}{(0.2325 - 25.7837)(0.2325 - 0.0419)} = 0.9857$$
$$|e_{31}|^2 = \frac{(0.0419 - 25.7489)(0.0419 - 0.04438)}{(0.0419 - 25.7837)(0.0419 - 0.2325)} = 0.0130$$

i.e., the same solution as obtained by means of the (differently rotated) eigenvectors of the coherency matrix.

V. Conclusion

The Cloude–Pottier mean alpha angle, $\bar{\alpha}$, can be determined by means of the first components of the eigenvectors $\boldsymbol{e}_i$ of the 3×3 Hermitian coherency matrix. These eigenvectors may be rotated by any angle ϕ_i, i.e., $\boldsymbol{e}_i$ may be replaced by $\boldsymbol{e}_i \exp(j\phi_i)$ and still be a solution to the eigenproblem.

Alternatively, $\bar{\alpha}$ may be calculated based on the eigenvalues of the coherency matrix and its first 2×2 minor by means of the so far little known EEI without calculating eigenvectors. This facilitates fast array-based computer implementation of the $\bar{\alpha}$ angle calculation.

MATLAB code with this array-based implementation will be made available from the author's homepage https://people.compute.dtu.dk/alan under "Publications".

References

[1] J.-S. Lee, M. R. Grunes, T. L. Ainsworth, L.-J. Du, D. L. Schuler, and S. R. Cloude, "Unsupervised classification using polarimetric decomposition and the complex Wishart classifier," *IEEE Trans. Geosci. Remote Sens.*, vol. 37, no. 5, pp. 2249–2258, Sep. 1999, doi: 10.1109/36.789621.

[2] S. R. Cloude and E. Pottier, "An entropy based classification scheme for land applications of polarimetric SAR," *IEEE Trans. Geosci. Remote Sens.*, vol. 35, no. 1, pp. 68–78, Jan. 1997, doi: 10.1109/36.551935.

[3] A. A. Nielsen, "Fast matrix based computation of eigenvalues and the Loewner order in PolSAR data," *IEEE Geosci. Remote Sens. Lett.*, vol. 17, no. 2, pp. 242–246, Feb. 2020, doi: 10.1109/LGRS.2019.2952202.

[4] K. T. Löwner, "Über monotone matrixfunktionen," *Mathematische Zeitschrift*, vol. 38, pp. 177–216, Dec. 1934. [Online]. Available: https://eudml.org/doc/168495

[5] S. Hensley, "The eigenvector-eigenvalue identity and radar polarimetry," in *Proc. IEEE Int. Geosci. Remote Sens. Symp. (IGARSS)*, Jul. 2021, pp. 2–5, doi: 10.1109/IGARSS47720.2021.9554916.

[6] P. B. Denton, S. J. Parke, T. Tao, and X. Zhang, "Eigenvectors from eigenvalues: A survey of a basic identity in linear algebra," *Bull. Amer. Math. Soc.*, vol. 59, no. 1, pp. 31–58, Jan. 2022, doi: 10.1090/bull/1722.

[7] A. Reigber *et al.*, "Very-high-resolution airborne synthetic aperture radar imaging: Signal processing and applications," *Proc. IEEE*, vol. 101, no. 3, pp. 759–783, Mar. 2013, doi: 10.1109/JPROC.2012.2220511.

[8] A. A. Nielsen, P. J. Connetable, H. Skriver, and K. Conradsen, "A version of the Cloude/van Zyl decomposition for full/quad pol synthetic aperture radar data," Tech. Univ. Denmark, Tech. Rep., Lyngby, Denmark, Apr. 2022, doi: 10.11581/DTU.00000237.

[9] J. J. van Zyl, "Application of Cloude's target decomposition theorem to polarimetric imaging radar data," *Proc. SPIE*, vol. 1748, pp. 184–191, Feb. 1993, doi: 10.1117/12.140615.

[10] J. J. van Zyl, M. Arii, and Y. Kim, "Model-based decomposition of polarimetric SAR covariance matrices constrained for nonnegative eigenvalues," *IEEE Trans. Geosci. Remote Sens.*, vol. 49, no. 9, pp. 3452–3459, Sep. 2011, doi: 10.1109/TGRS.2011.2128325.